OXFORD

Journal of Petrology, 2022, **63**, 1–14
https://doi.org/10.1093/petrology/egac056
Original Manuscript

Crystal-Liquid Segregation in Silicocarbonatite Magma Leads to the Formation of Calcite Carbonatite

K. R. Moore[1,*], A. E. Brady[2] and A. Costanzo[3]

[1]Camborne School of Mines, University of Exeter, Penryn Campus, Cornwall TR10 9FE, UK
[2]iCRAG, SFI Research Centre in Applied Geosciences, University College Dublin, Dublin D04 V1W8, Ireland
[3]School of Natural Sciences, National University of Ireland Galway, Galway H91 TK33, Ireland

*Corresponding author. Telephone: 0044 (0)1326 255693. E-mail: k.moore@exeter.ac.uk

Abstract

A suite of silicocarbonatite and lamprophyre rocks from SW Ireland, with mantle affinity and primitive composition, are used as a proxy for parental carbonated silicate magmas to model early magmatic evolution. Reconstruction of volatile ratios is validated using global occurrences. At 1200°C, the point at which melts transition from ionic liquids with exceptionally low viscosity (0.06 PaS) to covalently polymerised liquid (viscosity up to 1.3 PaS) is 33 mol% SiO_2. Incremental and significant increase in magma density accompanies magma ponding, due to dehydration of magmas from model molar $CO_2/(CO_2 + H_2O)$ of 0.60 in plutonic settings to 0.75 for initial subvolcanic magmas. Magma-crystal density differences dictate that repeated influxes of magmas into an inflating magma chamber sustain a mechanical boundary layer between dense (silicate and oxide) mineral layers and a calcite ± phlogopite flotation assemblage. The range of critical CO_2 concentration at which calcite floats (10–13 wt% CO_2) may be extended by the presence of additional volatiles and fluid bubbles. The model accommodates a range of phenomena observed or inferred for alkaline/carbonatite complexes, including the following: 1, a growing calcite-dominated flotation assemblage with an apparently early magmatic mineralisation; 2, a residual liquid with high concentrations of incompatible metals; 3, variable carbonatite–pyroxenite–phoscorite rock relations; and 4, multiple phases of overprinting metasomatism.

Keywords: mechanical boundary layer, magma rheology, flotation, crystallisation, carbonatites

INTRODUCTION

Observations of the cumulate plutonic carbonatites and their surrounding fenites suggest that neither intrusive nor volcanic rocks fully represent the compositions of parental melts and fluids (Kamenetsky *et al.*, 2021). Experimental petrology in synthetic systems demonstrates that the possible parental melts from the mantle ranges from dolomite carbonatite to carbonated silicate compositions (Dalton & Presnall, 1998; Moore & Wood, 1998; Girnis *et al.*, 2005; Gudfinnsson & Presnall, 2005; Moore, 2012; Massuyeau *et al.*, 2015). However, case study-based research shows both that reactive assimilation of silica by carbonatites can arise from wall-rock entrainment in the crust (Drüppel *et al.*, 2005; Chmyz *et al.*, 2022) and that carbonatitic lamprophyres can be unaffected by contamination in either high or low pressure regimes (Vichi *et al.*, 2005; Stoppa *et al.*, 2014). In this manuscript, we present evidence that silicocarbonatite (carbonatites with more than 20% silicate minerals) and lamprophyre rocks from the Beara Peninsula in SW Ireland are sufficiently free of contamination to be a useful proxy for natural parental compositions, and suitable for modelling of early magmatic evolution.

Fractionation is an important petrogenetic process in the formation of cumulate carbonatites, the evolution of liquids that subsequently undergo immiscible separation, and the generation of residual liquids or fluids that are rare earth element (REE)-enriched (Watkinson & Wyllie, 1971; Smith *et al.*, 2016; Anenburg *et al.*, 2021; Yaxley *et al.*, 2021). Silicocarbonatite and lamprophyre have been described as important parental liquid compositions or compositions on the carbonatite fractionation path (Middlemost, 1990; Mitchell, 2005; Vichi *et al.*, 2005; Moore, 2012). Calcite, mica and apatite are important phases in the fractionation of a volatile enriched magma, crystallising over a large compositional and temperature range (Harmer & Gittins, 1997; Vichi *et al.*, 2005; Weidendorfer *et al.*, 2017; Giebel *et al.*, 2019), and an association with pyroxene and mica-dominated cumulate rocks is significant (e.g. Chakmouradian & Zaitsev, 2004; Woolley & Kjarsgaard, 2008; Chmyz *et al.*, 2022). The behaviour of carbonate-rich magmas at the point of emplacement in

Received: March 2, 2022. **Revised:** June 15, 2022. **Accepted:** June 16, 2022

the upper crust and the fractional relationship between silicate and carbonate cumulates is obscured by complex multi-stage evolutionary histories. Here, we use natural silicocarbonatite and associated lamprophyre magmatic compositions to model magma rheology and crystal settling.

Experimental determinations of magma rheology necessarily use end-member or simple synthetic compositions because of the propensity of carbonated silicate liquids to separate at low pressures. Nevertheless, they explain how low density and viscosity, small-fraction magmas undergo rapid separation from source regions, rapid ascent to the crust, and rapid crystal settling (Treiman & Schedl, 1983; Hunter & McKenzie, 1989; Genge *et al.*, 1995b; Kono *et al.*, 2014; Stagno *et al.*, 2018). Small-fraction carbonatite liquids can evolve by reaction with wall-rock in the mantle or crust with concomitant volatile exsolution or fractionation (Freestone & Hamilton, 1980; Green & Wallace, 1988; Gittins, 1989; Anenburg & Mavrogenes, 2018), which reduce the thermal capacity of magmas. The scale and rate of processes are difficult to reconcile with ponding to form significant silicate and carbonate-dominated cumulate rocks, even using lithosphere focussing of melts derived from a large area of mantle (Bailey, 1985; Gittins, 1989; Dalton & Wood, 1993; Lee & Wyllie, 1997; Woolley & Bailey, 2012). We combine the field evidence for emplacement of silico-carbonatite and lamprophyre rocks with the chemical modelling of magma rheology to postulate on the geometry and nature of an inflating magma chamber that can accommodate incrementally injected small-fraction magmas. A focus on the start of magma fractionation within the crust has broader implications: it may help to understand paths of cumulate rock formation and magmatic evolution, and thereby the extreme variability in carbonatite complexes, and rock associations.

GEOLOGY

The subvolcanic intrusions in the Beara Peninsula (western County Cork, SW Ireland) investigated were 1 diatreme, 2 pipes, 12 dykes and 11 sills (Fig. 1a). The intrusions are dated to a 17-million-year time interval straddling the end of Variscan deformation, from 314 to 297 Ma (Quinn *et al.*, 2005). The magmatism follows a recent period of mantle metasomatism at 318 Ma in a source region greater than 75 km deep (Pracht & Kinnaird, 1995; Pracht & Timmerman, 2004). Brady & Moore (2012) ascribed the zoned silicocarbonatite breccia pipe at Cahermore (1p3; Fig. 1a) to a near-primary magma produced by partial melting in metasomatised mantle at physical conditions between those in which primary dolomite carbonatite and ultramafic magmas of high-pressure originate.

Carbonatites and strongly carbonated silicate rocks with only minimal signs of contamination by crustal xenolith entrainment were selected for modelling. Field relations show that injection of small volumes of magma was episodic (Figs 1 and 2): repeated injection acted to inflate intrusions, by dyke-in-dyke injection (Fig. 2a), or following rough fractures and dyke/sill margins (Figs 1b, c and 2c). In some instances, the first magma was rapidly emplaced and transported mantle materials (Figs 1d and 2c, d), becoming consolidated before injection of a second magma that has a fluidised appearance and sometimes utilised fractures (Figs 1b, c and 2b, c). Figure 2a shows an intrusion that comprises a rock with cleavage on its margins and a central rock with no cleavage, representing injection of a magma that split and inflated the intrusion after the stress field had changed. The field evidence for the time interval between injection of magmas in intrusions precludes an origin by co-genetic immiscible separation.

Settlement of a xenolith population to the base of a sill (Figs 1d and 2d) implies a diminished force of transport. The settling of strongly autometasomatised mantle xenoliths is explained by experiments that have measured a decrease in magmatic overpressure of up to 60% at the moment of sill inception (Kavanagh *et al.*, 2006; Daniels *et al.*, 2012), such that the potential for magma to transport mantle xenoliths is reduced. The decrease in magmatic overpressure is accompanied by a reduction in PH_2O of the magma (Hort, 1998; Kavanagh *et al.*, 2015). It explains liquidus perturbations that increase the crystal fraction (Hort, 1998; Kavanagh *et al.*, 2015) and autometsomatism of the xenoliths (Fig. 2d), which are now dominated by hydrous talc-serpentine assemblages. The point of emplacement is interpreted as proximal to a central feeder area of magmas with strong mantle affinity in a dyke-sill-pipe system at White Ball Head (Fig. 1a).

The carbonated silicate intrusions are cross-cut by, and in turn cross-cut, phonolite and trachyte intrusions. It is possible that there are two source regions for magma production. It is also possible that magmas can either ascend rapidly without extensive fractionation, or pond, or have an extensive petrogenetic history. The compositions of lithologies that may represent residual magmatic systems are not used for the purposes of modelling the start of fractionation. The important characteristics of the geology that are factored in the geometry of the final model are (1) episodic addition to, or inflation of, intrusions by mantle-derived magmas; (2) decrease in transport velocity of magmas at the point of sill inception; and (3) accompanying release of volatiles.

ANALYTICAL METHODS

Representative samples were collected from 1 diatreme, 2 pipes, 11 dykes and 6 sills (not all intrusions were accessible for sampling). Trachyte and phonolite samples are not used for the modelling. Samples of breccia were also not used for modelling where crustal contamination was inevitable, e.g. the breccia pipe 2p3 on White Ball Head (Fig. 1a). Weathered crusts on rock samples were

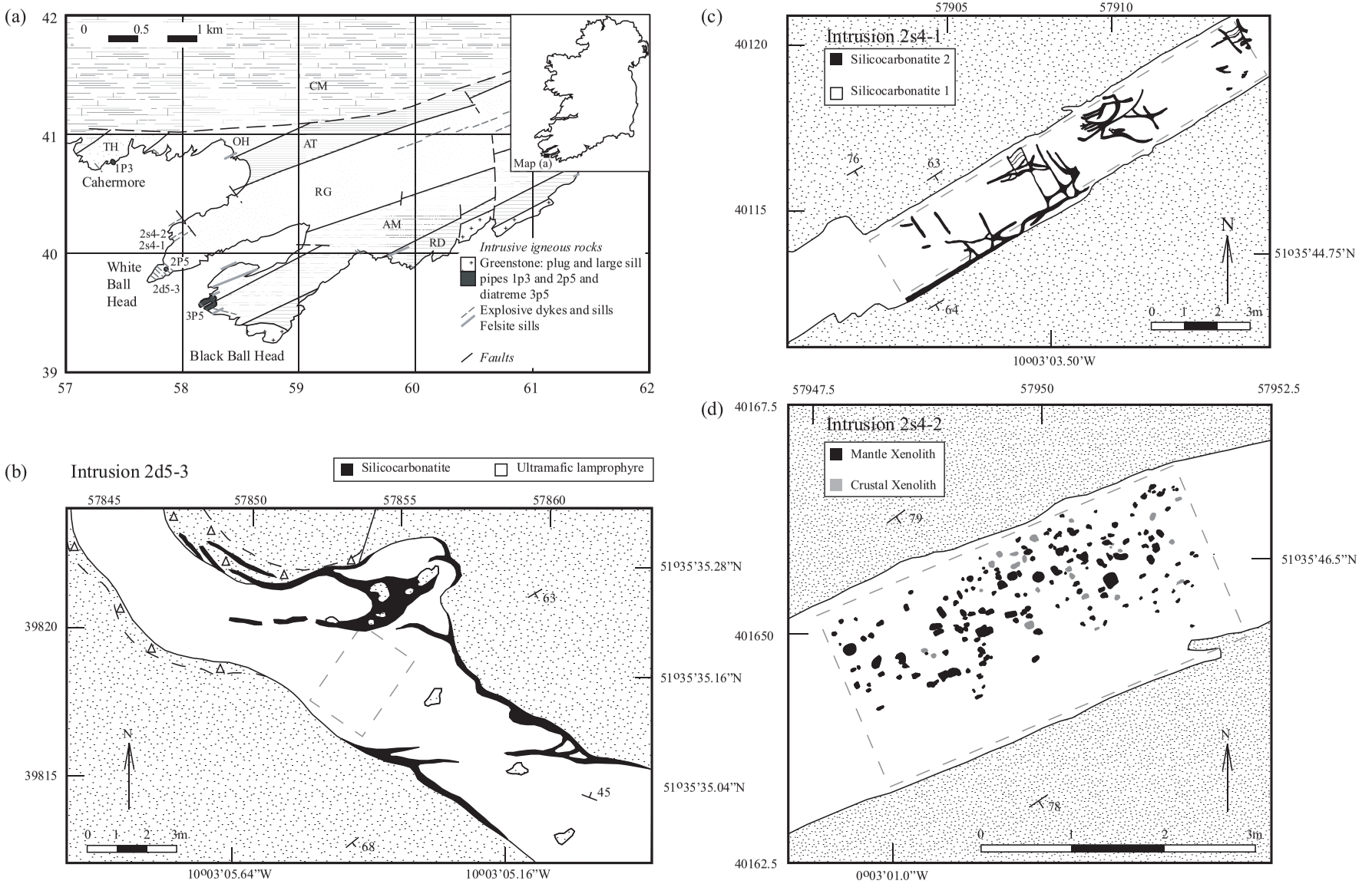

Fig. 1. Geological maps of the subvolcanic intrusions of the Beara Peninsula, western County Cork, SW Ireland. (a) 1 diatreme and 2 pipes (p), 12 dykes (d) and 11 sills (s) after Brady & Moore (2012) intrude the stratigraphy of Pracht (1994)*. (b) An explosive dyke (3d5) brecciated country rock, transported mantle xenocrysts and was intruded by late stage magmas. (c) Sill 2s4-1 contains mantle xenocrysts; a later pulse of magma utilised interfaces between the former intrusion and country rock, and rough jointing or flow lines within the former intrusion. (d) Mantle and crustal xenoliths rapidly settled out of a magma in sill 2s4-2 (way-up to SSE). Both the longitude and latitude co-ordinates and the Irish National Grid co-ordinates (V) are shown for reference. *CM, TH, OH, AT, RG, AM, RD represent the Late Devonian to Early Carboniferous formations that are dominated by sandstones and mudstones.

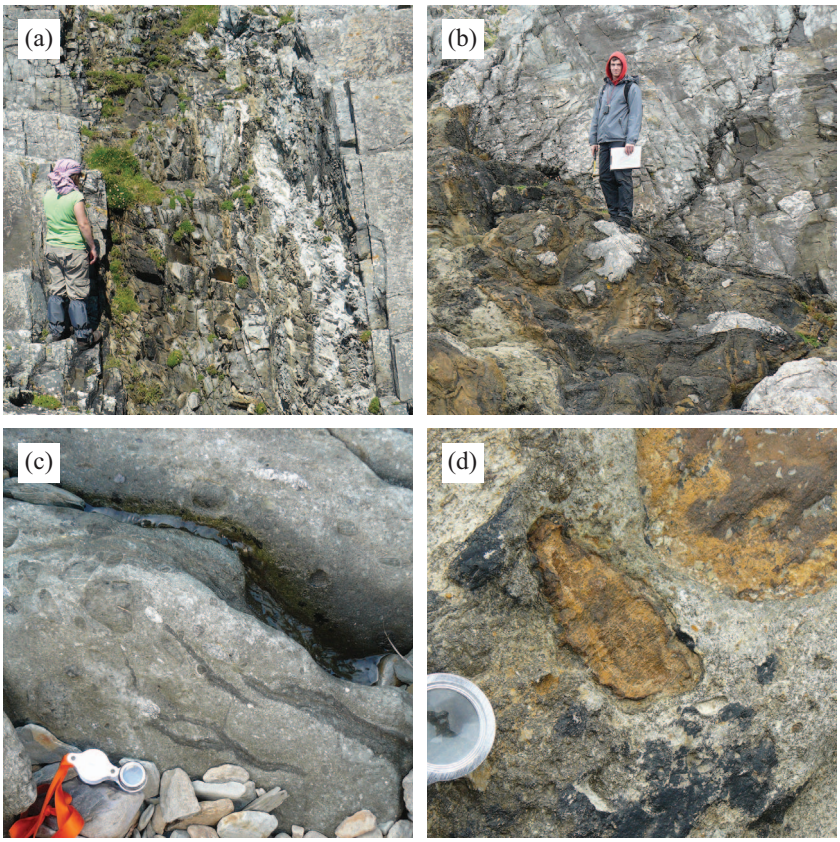

Fig. 2. Field photographs depicting intrusive relations. (a) Dyke-in-dyke injection (2d5-2), where the syn-Variscan early intrusion has cleavage and the post-Variscan central intrusion is without cleavage. (b) Explosive blow on the margin of dyke 2d5-3, incorporating large blocks of country rock and brecciating the host-rock walls of the dyke. (c) Late stage silicocarbonatite magma intrudes alkaline ultramafic magma in sill 2s4-1, which has entrained mantle xenocrysts. (d) The mantle xenoliths in 2s4-2 are subject to extreme metasomatism.

removed as far as possible, during rock cutting in the field and/or prior to laboratory preparation.

Major element whole-rock compositions were analysed by OMAC Laboratories in Loughrea, Co. Galway, using the Perkin Elmer Optima 3000DV dual view ICP Atomic Emission Spectrometer (ICP-AES). A complete suite of 29 trace elements and the REEs were analysed using the X-Series Thermo Electron Quadrupole Inductively Coupled Plasma Mass Spectrometer (ICP-MS). The certified reference materials NIM-N (norite), SY-3 and SY-4 (syenite), compositions as cited by Govindaraju (1994), were analysed to clarify the accuracy of the preparation method and record any drift or changes in results between the sample batches.

Stable isotope analyses were carried out at the Unitat de Medi Ambient of the Serveis Científico-Tècnics, Universidad de Barcelona. Samples were analysed using an automated Kiel Carbonate Device attached to a Thermal Ionization Mass Spectrometer Thermo Electron (Finnigan) MAT-252. The average sample weight for each single rock analysed was 60 ± 10 μg. Isotope measurements were calibrated to the Pee Dee Belemnite (PDB) scale by means of the International Atomic Energy Agency (IAEA) NBS-18 and NBS-19 carbonate isotope standard. Values are expressed as per mil differences relative to the PDB and Standard Mean Ocean Water (SMOW) standards.

WHOLE-ROCK CHEMISTRY

Lithologies excluded from the modelling had visible and extensive contamination due to entrainment of country rocks (e.g. pipe 2p3; Fig. 1a), and high SiO_2 (up to 53.61 wt%) and Al_2O_3 (up to 12.96 wt%), moderately high Na_2O concentrations (2.53 wt%) and low K_2O contents (0.92 wt%). The major element chemistry of rocks used for modelling is presented in Table 1. The rocks have groundmass carbonates spanning a large range of compositions: calcite, dolomite, ferroan dolomite, ankerite and magnesite. The most magnesium-rich intrusions classify chemically as either silicocarbonatite or ultramafic lamprophyre (Fig. 3). The mineralogy, described in detail by Brady (2010), confirms affinity to two lamprophyre branches: ultramafic lamprophyres and alkaline lamprophyres, which are more aluminium rich. There are no lithologies that have chemistry similar to co-genetic immiscible carbonate–silicate pairs.

The silicocarbonatite intrusions are pipe 1p3 and sills 2s4-1 and 2s4-2 (Figs 1 and 2). The 1p3 dolomite silicocarbonatite has comparatively low CaO (10.26 wt%) but high MgO, Fe_2O_3 and SiO_2 contents (14.30 wt% 12.49 wt% and 31.80 wt%, respectively). The abundance of alkalis is conspicuously low (0.16 wt% K_2O and 0.15 wt% Na_2O). Sill 2S4-1 has the lowest SiO_2 (27.32 wt%) but very high CaO (17.07 wt%) consistent with a petrographic classification

Table 1: Whole-rock major (wt%) and trace element (ppm) chemistry of Beara intrusions, this study and Pracht (1994): pipe and diatreme, xenolith- and xenocryst-bearing sills and dykes, xenolith- and xenocryst-absent tuff dykes

Intrusion type	**Pipe**		**Diatreme**				**Sills**				**Dykes**					
Sample no.:	1p3	3p5.1	3p5.3	3p5.4	91–58*	90–22*	2s4-1	2s4-1b	2s4-2	1d3	2d5-3	3d5	3d6	6d5	3d3	2d3
SiO_2	31.8	30.11	43.5	34.17	33.95	34.177	27.32	33.45	44.13	27.73	33.3	35.05	31.68	35.37	33.03	39.84
TiO_2	2	2.16	2.54	2.15	3.38	2.52	2.27	2.58	2.43	2.79	1.39	3.17	3.23	2.79	1.95	2.17
Al_2O_3	6.36	7.15	8.78	7.17	10.17	8.92	6.6	7.38	9.14	7.72	5.21	9.86	17.11	15.51	17.07	13.86
FeO^T	11.24	10.76	11.1	11.12	13.87	12.04	11.41	12.42	11.62	10.29	9.74	11.66	19.72	9.83	8.52	10.19
MnO	0.36	0.37	0.26	0.24	0.302	0.24	0.27	0.3	0.31	0.23	0.32	0.25	1.36	0.69	1.24	0.42
MgO	14.3	12.15	14.71	14.26	11.48	13.67	12.21	18.27	14.21	10.81	18.7	10.99	4.16	3.1	3.44	4.8
CaO	10.26	18.21	10.06	16.86	14.63	11.32	17.07	8.3	3.98	14.81	9.36	11.91	5.46	13.35	10.27	7.89
Na_2O	0.15	0.51	0.61	0.29	1.11	0.24	0.76	0.18	0.16	0.56	0.16	0.54	0.84	0.97	1.9	1.49
K_2O	0.16	0.88	2.69	0.43	2.54	0.04	2.39	1.28	0.06	0.17	0.31	0.39	2.16	1.92	2.94	1.75
P_2O_5	1.18	2.63	1.27	2.23	1.51	1.02	2.61	1.55	0.93	1.02	0.35	1.54	0.76	0.57	0.82	0.59
LOI	19.83	11.22	4.16	8.3	8.14	17.37	14.3	10.52	8.83	21.35	19.6	12.03	9.29	14.72	15.07	13.53
Total	97.64	96.15	99.68	97.22	101.08	101.56	97.21	96.23	95.80	97.48	98.44	97.39	95.77	98.82	96.25	96.53
Mg #	69.4	66.8	70.3	69.6	59.6	66.9	65.6	72.4	68.6	65.2	77.4	62.7	27.3	36	41.9	45.6
LFSE																
Rb	1.35	71.4	22.5	41.1	-	-	196	124	1.84	10	28.6	24.8	108	102	178	97.3
Ba	49.4	442	477	160	-	-	1627	744	16.2	79.7	150	878	308	276	332	314
Sr	1043	1634	933	1589	-	-	2259	906	525	536	979	880	114	239	169	236
HFSE																
Th	10.6	31	1.8	15.2	-	-	22.5	11.3	7.83	15.5	3.6	15.08	10.6	6.7	11.3	8.7
U	2.63	6.4	0.8	5.52	-	-	6.66	2.8	2.25	3.2	1	3.32	2.4	1.6	3.14	2.36
Nb	92.8	146	39.6	108	-	-	129	117	85.7	127	47.7	120	118	70.7	127	80.4
Ta	4.52	4.51	2.4	4.21	-	-	4.29	5.6	4.41	7.1	2.6	5.3	6.8	4.2	5.96	4.64
Pb	12.1	3.22	40.4	-	-	-	7.61	-	6.92	55.2	4.7	24.9	38	6.2	14.8	3.55
Zr	155	164	156	153	-	-	162	165	163	209	93	236	351	232	300	235
Hf	4.23	3.94	5	2.62	-	-	3.82	3	4.72	5	2	6.17	8	6	6.71	5.77
Y	22.4	54	23.7	60.8	-	-	53.8	33.8	24.6	29.1	12.5	28.7	41.4	32.4	32.3	26.4
REE																
La	68.8	184	23.9	185	-	-	168	88.8	55	103	29.7	90.8	75.1	45.2	64.5	49.6
Ce	130	342	55.7	309	-	-	305	167	105	188	55.9	170	145	91.1	136	95.6
Pr	14.8	37.5	8	40.5	-	-	34	19.1	12.2	21.5	6.5	19.3	16.9	10.9	15.9	10.8
Nd	56.9	140	38.6	148	-	-	128	72.7	48.4	79.5	25.4	73.8	63.3	41.6	60.9	40.7
Sm	10.4	24.2	9.3	28.7	-	-	22.5	13.4	9.93	14.1	5	13.4	13.1	8.7	12.8	7.54
Eu	2.97	6.48	3.7	7.17	-	-	6.94	4.2	2.67	4.1	1.5	4.08	4.2	2.7	3.66	2.56
Gd	9.2	21.6	8.4	25.5	-	-	21	11.1	8.3	12	4.2	11.4	12.3	8.4	11	7.5
Tb	1.22	2.66	1.1	2.07	-	-	2.71	1.4	1.15	1.5	0.5	1.53	1.7	1.3	1.48	1.07
Dy	5.41	12.5	5.8	10.7	-	-	12.1	7.2	5.57	6.6	2.7	6.88	8.2	6.4	6.92	5.35
Ho	0.92	2.1	1	2	-	-	2.12	1.2	0.95	1.1	0.5	1.12	1.5	1.2	1.27	1.02
Er	2.32	5.7	2.4	6.68	-	-	5.68	3	2.59	2.6	1.2	2.86	4.1	3	3.65	3
Tm	0.27	0.6	<0.5	0.48	-	-	0.69	0.4	0.28	0.3	0.1	0.31	0.6	0.4	0.45	0.36
Yb	1.46	3.5	1.6	4.03	-	-	3.49	2.1	1.68	1.7	0.9	2.05	3.2	2.3	3.01	2.21
Lu	0.2	0.6	<0.5	0.38	-	-	0.5	0.3	0.3	0.2	0.1	0.3	0.5	0.3	0.5	0.4
∑REE	305	783	160	771	-	-	714	392	254	437	134	398	350	224	322	228
La/Lu	313	335		482	-	-	358	317	204	443	256	349	158	133	143	134
Transition metals																
Cr	847	411	16	714	-	-	348	883	475	272	1295	221	212	120	10	170
Co	59.7	42	84.9	-	-	-	79.8	-	44.8	57.2	57.5	52	212	27.6	51.2	25.8
Ni	611	274	86	-	-	-	545	-	180	195	529	221	211	54.9	20.6	101
Sc	20.4	19.9	48.3	24.6	-	-	33.6	22	22.1	18	17	24.8	23	16	3.88	19.9
V	210	227	414	202	-	-	326	193	258	203	138	307	227	165	52	204

FeO^T = total iron. Mg # = (Mg-number assuming all iron as Fe^{2+}) = $100(Mg/(Mg + Fe^{2+}))$ in atomic units. -, not analysed.*Pracht (1994)

(Brady, 2010) as calcite carbonatite. The subordinate second melt (2S4-1b) observed in the sill 2S4-1 contains higher MgO (18.27 wt%), SiO_2 (33.45 wt%) and much lower CaO (8.30 wt%). Sill 2s4-2 contains higher SiO_2 (44.31 wt%) and very low CaO (3.98 wt%) compared with sill 2s4-1. 2S4-1 and 2S4-2 have high Fe_2O_3 (12.68 and 12.91 wt%, respectively) and MgO (12.21 and 14.21 wt%, respectively). On the Al_2O_3-CaO-MgO discrimination ternary diagram for lamprophyres, sill 2s4-1 plots within the ultramafic lamprophyre field whereas sill 2s4-2 sits outside the two fields (Fig. 3a).

Intrusions that classify as alkaline ultramafic lamprophyres are dykes 1d3, 3d5 and 2d5-3 and diatreme pipe 3p5 (Fig. 3a). The presence of Cr-spinel, Mn-rich ilmenite and the abundance of Sr-rich groundmass calcite support an ultramafic lamprophyric affinity. The diatreme pipe 3p5 has very low but varying SiO_2 (30.11–43.5 wt%) and Al_2O_3 (7.15–11.33 wt%). MgO concentration

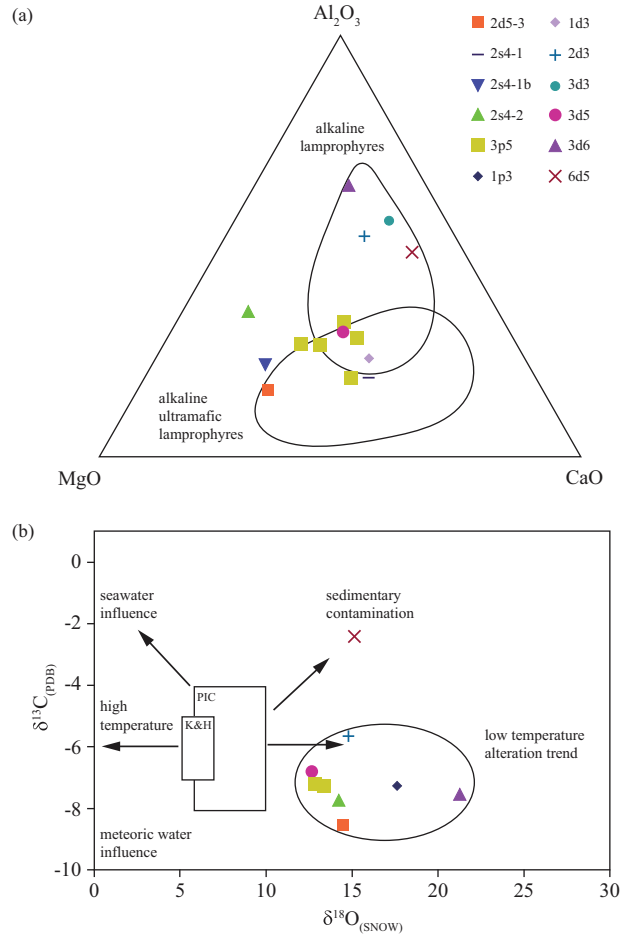

Fig. 3. Representative whole-rock and stable isotope chemistry of the primary sample set used for modelling. (a) Classification of subvolcanic intrusions of the Beara Peninsula using the Al_2O_3-CaO-MgO (wt%) ternary discrimination diagram (after Rock, 1987). There is a continuum of alkaline ultramafic intrusions from silicocarbonatite sills, across the compositions of the diatreme pipe 3p5, into the overlap field between ultramafic and alkaline lamprophyres. There alkaline lamprophyre dykes have more evolved compositions. (b) Oxygen and carbon isotope ratios in carbonates from silicocarbonatites, alkaline ultramafic lamprophyres and lamprophyres (relative to SMOW and PDB). PIC and K & H represent the isotopic compositions of primary unaltered carbonatites as proposed by Taylor *et al.* (1967) and Keller & Hoefs (1995), respectively.

is high (11.97–14.71 wt%) and CaO concentration (10.06–18.21 wt%) is also high, but variable. The compositional variation corresponds with the fluidised nature of the intrusion, such that samples likely represent successive injections of magma (Gernon *et al.*, 2009). The composition is comparable with average ultramafic lamprophyres (Rock, 1991). Mg-numbers are high (57–70) and TiO_2 concentrations are also elevated (2.15–5.78 wt%). The alkaline ultramafic lamprophyre dykes contain high MgO (10.99–18.70 wt%), low Al_2O_3 (5.21–9.86 wt%) and low alkali concentrations. Low alkali concentrations (e.g. $Na_2O < 0.61$ wt% and $K_2O < 1.38$ wt% in 3p5) are, according to Tappe *et al.* (2006), characteristic for the ultramafic lamprophyre type aillikite.

Dykes 2d3, 3d5, 3d6 and 6d5 contain kaersutite, Ti-rich phlogopite and Ti-magnetite megacrysts and are classified as alkaline lamprophyres (Fig. 3a). The presence of abundant plagioclase feldspar in dyke 3d5 also supports an alkaline affinity, while diopside is common to both alkaline and ultramafic lamprophyres. The alkaline lamprophyre dykes have high Al_2O_3 (13.86–17.11 wt%) and low MgO (3.10–4.80 wt% MgO) concentrations. The group is also markedly potassic ($K_2O > Na_2O$, Table 1).

On the Al_2O_3-CaO-MgO discrimination ternary diagram for lamprophyres (Fig. 3a), the alkaline ultramafic group forms a continuum from silicocarbonatite compositions, across the compositions of the diatreme pipe 3p5, towards and into the overlap field for ultramafic and alkaline lamprophyres.

STABLE ISOTOPE CHEMISTRY

The stable isotope data for a selection of the Beara subvolcanic intrusions are summarised in Table 2 and Fig. 3b. Nearly all δ^{13} C_{PDB} values (−5.64 to −8.51‰) obtained for the selected Beara intrusions are comparable with the primary igneous carbonatite (PIC) box of Taylor *et al.* (1967), indicating a dominantly mantle-derived influence. An anomalous $\delta^{13}C$ result (−2.43 relative to C_{PDB}) for dyke 6d5 (Fig. 3b) is isotopically explained by sedimentary contamination (Santos & Clayton, 1995) although this is not apparent in the appearance of the rock, nor the major element chemistry, nor the modelling results. The extensive remobilisation of sedimentary carbonate for the rest of the Beara subvolcanic rocks is very unlikely because even completely recrystallised carbonate usually preserves sedimentary $\delta^{13}C$ (e.g. Demény & Harangi, 1996; Hegner *et al.*, 2020) and because only one of the host formations (RD Reenydonagan Formation; Fig. 1a) includes calcareous mudstones.

The $\delta^{18}O$ values vary from 12.64 to 18.57‰. The most primitive end of a near-primary cluster of $\delta^{13}C$ and $\delta^{18}O$ data is defined by the calcite-rich lamprophyre diatreme (3p5) and dyke (3d5), which have field and chemical characteristics indicating that they were rapidly emplaced from the mantle. Nevertheless, they are somewhat removed isotopically from the PIC box. The high $\delta^{18}O$ end of the correlation is constrained by the xenolith- and xenocryst-free dyke 3d6, which has chemical and mineralogical characteristics indicating some greater extent of crustal residency and magmatic evolution. Assimilation of significant silicate host rocks (dominantly sandstones and mudstones) might be expected to explain this result. However, silicocarbonatite 1p3 also has elevated $\delta^{18}O$ and preserves mantle xenocrysts in preference to crustal xenoliths, and is it unlikely that crustal material was selectively consumed by magma during rapid emplacement, while mantle material was preserved.

Breccia pipe 2p3 (White Ball Head; Fig. 1a) was not included in the data or modelling because it has excessively high Al_2O_3 and SiO_2 concentrations, being dominated by clasts of host rock. There is no positive correlation between $\delta^{18}O$ values and SiO_2 concentrations

Table 2: C- and O-isotope compositions of carbonate minerals in a selection of pipes (p), dykes (d) and sills (s) from the Beara Peninsula, relative to SMOW and PDB

Intrusion no:	$\delta^{13}C$ (‰. PDB)	$\delta^{18}O$ (‰. SNOW)	Carbonate
Silicocarbonatites			
1p3	−7.26	17.56	Ferroan dolomite
2s4-2	−7.77	14.23	Ferroan dolomite
Alkaline Ultramafic Lamprophyres			
3p5-2	−7.26	13.36	Calcite
3p5-3	−7.20	12.90	Calcite
2d5-3	−8.51	14.38	Calcite
3d5	−6.80	12.64	Calcite
Alkaline Lamprophyres			
2d3	−5.64	14.82	Ankerite
3d6	−7.59	21.26	Ankerite
6d5	−2.43	15.13	Ankerite

for rocks 1p3, 2d3 or 3d6, which would indicate similar assimilation of crustal silicate rocks. Variable Al_2O_3 concentration and Mg number (Table 1) are better explained by fractionation than by crustal assimilation, such that the $\delta^{18}O$ composition of rocks is interpreted as the result of low-temperature alteration. Overall, the isotope data suggest that the low-temperature alteration has not affected the major element chemistry and that screening of samples for the purpose of modelling primitive (silicocarbonatite and ultramafic lamprophyre), and somewhat fractionated (alkaline lamprophyre) magmas, was successful.

MAGMA VISCOSITY

In order to constrain input data in the first instance, whole-rock data from the primary data set have $32.7 < \text{mol \% } SiO_2 < 54.5$ and were used to estimate the non-Arrhenian Newtonian viscosity. The viscosity model of Giordano *et al.* (2008) reliably predicts the viscosities of melts from 10^{-1} to 10^{14} PaS, such that it has been successfully used to approximate carbonated melts (Valentini & Moore, 2009).

The viscosity of intruding magmas is calculated using the selected rock compositions from the Beara Peninsula as a proxy and an established method based on the general VFT Vogel–Fulcher–Tamman equation (i) for temperature dependence of viscosity (Giordano *et al.*, 2008):

$$\log\eta = A + \frac{B}{T(K) - C}, \qquad \text{(i)}$$

where A, B and C are adjustable parameters, including the pre-exponential factor, pseudo-activation energy, and the VFT-temperature, respectively. The data (Table 3) are plotted in Fig. 4. Although the depolymerising effect of CO_2 is ignored by the model, one of the whole-rock compositions from the Beara Peninsula contains $SiO_2 < 33$ mol%, such that it should behave as an ionic liquid (Masson *et al.*, 1970; Masson, 1972). The whole-rock composition with molar $CO_2/(CO_2 + H_2O)$ or $Vr = 0.75$ produces a calculated magma viscosity that

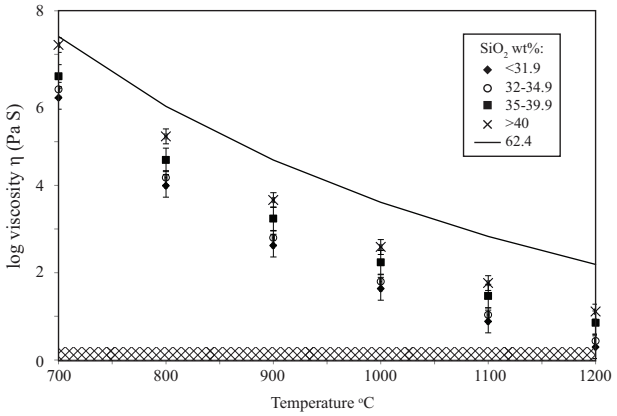

Fig. 4. Relationship between viscosity and temperature for carbonated liquids. The viscosities of carbonate-free granodiorite (solid line) and silica-absent carbonate ionic liquids (cross-hatched area) are shown for reference. The data for each range of silica concentrations are mean viscosities calculated using the whole-rock analyses of intrusions in the Beara Peninsula and error bars are 1 standard deviation from the mean.

is comparable with ionic liquids at high temperatures. The rest of the rock compositions have $SiO_2 > 33$ mol%, such that silica liquids behave covalently and SiO_2 concentration is the dominant control on viscosity. Viscosity increases by 0.59–2.02 PaS for every 100°C fall in temperature, with the largest increase in viscosity at lowest magmatic temperatures as predicted by the model, such that the difference between carbonated magmas and silicate magma (as depicted using the carbonate-free granodiorite composition; Giordano *et al.*, 2008) is reduced at lower temperatures.

The results show that melts with <33 mol% SiO_2 at high temperatures (1200°C) have exceptionally low viscosities (0.06 PaS) and behave as ionic liquids similar to a pure carbonate melt with high thermal conductivity (Masson *et al.*, 1970; Treiman & Schedl, 1983; Wolff, 1994; Genge *et al.*, 1995a; Dobson *et al.*, 1996; Kono *et al.*, 2014; Vuilleumier *et al.*, 2014; Stagno *et al.*, 2018). Above 33 mol% SiO_2, magmas behave as a covalently polymerised liquid, with viscosity up to 1.3 PaS, similar to alkali basalt.

Table 3: Representative outputs of modelling using the primary data set of rock compositions from SW Ireland. The effect of temperature is demonstrated for viscosity outputs over the full 700–1200°C range modelled. The viscosity data is not P-sensitive and can apply to plutonic settings. The results of density modelling are given for a temperature of 900°C: a variation of ±100°C produces a change in density of less than 0.02 g/cm^3. Density data is P-sensitive and applies to subvolcanic and shallow plutonic settings only (81 MPa equivalent to 2.5 km depth). Crystal settling rates were calculated for olivine, pyroxene, magnetite, apatite, phlogopite and calcite, over the full temperature range. Olivine, pyroxene and magnetite settling rates are not included here, because they are not significantly affected by the CO_2 concentration of magmas: minimum settling rates are 0.4 cm/sec for olivine and pyroxene and 1.5 cm/sec for magnetite. Crystal settling data is presented for a 900°C system and a 1 mm size of crystal.

Sample	1p3	3p5-1	3p5-3	3p5-4	91-58	90-22	2s4-1a	2s4-1b	2s4-2	1d3	2d5-3	3d5	3d6	6d5	3d3	2d3
CO_2 wt%	17.45	9.87	3.66	7.30	7.16	15.29	12.59	9.26	7.77	18.79	17.25	10.59	8.18	12.96	13.26	11.91
Viscosity (Pa S) for Vr = 0.75																
700.00	6.05	5.95	7.46	6.49	6.44	5.93	5.68	6.35	6.97	5.90	6.10	6.44	6.46	6.44	5.88	6.61
800.00	4.17	3.86	5.17	4.31	4.18	3.96	3.67	4.31	5.07	3.87	4.22	4.42	4.37	4.47	4.08	4.85
900.00	2.86	2.47	3.61	2.85	2.69	2.61	2.33	2.92	3.71	2.51	2.90	3.02	2.95	3.11	2.81	3.58
1000.00	1.89	1.47	2.49	1.81	1.64	1.63	1.36	1.90	2.69	1.52	1.93	2.00	1.91	2.10	1.86	2.61
1100.00	1.14	0.72	1.63	1.02	0.85	0.89	0.63	1.13	1.89	0.78	1.18	1.23	1.13	1.33	1.13	1.84
1200.00	0.55	0.14	0.96	0.40	0.24	0.30	0.06	0.52	1.25	0.20	0.59	0.61	0.52	0.71	0.55	1.22
Density (g cm^{-3}) for 900°C																
Vr = 60	2.26	2.58	2.71	2.64	2.63	2.31	2.46	2.58	2.54	2.24	2.26	2.47	2.61	2.32	2.35	2.35
Vr = 0.75	2.46	2.72	2.76	2.75	2.74	2.49	2.62	2.72	2.65	2.46	2.46	2.61	2.74	2.47	2.51	2.54
Vr = 0.86	2.58	2.80	2.79	2.81	2.80	2.59	2.72	2.79	2.71	2.58	2.57	2.69	2.80	2.56	2.60	2.57
Vr = 0.92	2.64	2.84	2.81	2.84	2.82	2.65	2.77	2.83	2.74	2.65	2.63	2.73	2.83	2.60	2.65	2.62
CRYSTAL SETTLING (cm sec $^{-1}$)																
Phlogopite																
Vr = 0.6	0.27	0.13	0.04	0.08	0.09	0.26	0.21	0.11	0.11	0.31	0.26	0.17	0.10	0.27	0.29	0.22
Vr = 0.75	0.17	0.04	0.01	0.02	0.03	0.17	0.10	0.04	0.06	0.19	0.17	0.09	0.03	0.15	0.15	0.10
Vr = 0.86	0.10	0.00	0.00	−0.01	0.00	0.10	0.04	0.00	0.03	0.12	0.11	0.04	0.00	0.09	0.08	0.08
Vr = 0.92	0.07	−0.02	−0.01	−0.02	−0.02	0.07	0.01	−0.02	0.02	0.07	0.07	0.02	−0.02	0.07	0.05	0.05
Apatite																
Vr = 0.6	0.51	0.40	0.22	0.32	0.35	0.52	0.50	0.33	0.30	0.59	0.49	0.40	0.35	0.54	0.60	0.45
Vr = 0.75	0.40	0.29	0.18	0.23	0.25	0.42	0.37	0.25	0.22	0.46	0.40	0.29	0.23	0.36	0.38	0.28
Vr = 0.86	0.32	0.22	0.15	0.18	0.20	0.34	0.29	0.19	0.18	0.36	0.33	0.23	0.17	0.27	0.27	0.23
Vr = 0.92	0.26	0.17	0.13	0.15	0.16	0.28	0.23	0.15	0.15	0.29	0.27	0.19	0.13	0.22	0.21	0.19
Calcite																
Vr = 0.6	0.34	0.12	0.00	0.06	0.07	0.33	0.24	0.10	0.11	0.40	0.33	0.19	0.08	0.33	0.35	0.26
Vr = 0.75	0.19	−0.01	−0.03	−0.03	−0.02	0.18	0.08	−0.01	0.04	0.22	0.19	0.07	−0.02	0.17	0.15	0.10
Vr = 0.86	0.10	−0.07	−0.05	−0.07	−0.06	0.09	−0.01	−0.06	0.00	0.11	0.10	0.01	−0.06	0.09	0.07	0.07
Vr = 0.92	0.05	−0.09	−0.05	−0.08	−0.07	0.04	−0.04	−0.07	−0.01	0.05	0.06	−0.01	−0.07	0.06	0.03	0.04

MAGMA DENSITY

Magma density calculations follow established methods (Bottinga & Weill, 1980), but incorporate thermal expansion and compressibility data for CO_2, where

$$\rho = \sum_i Y_i V_i, \quad \text{(ii)}$$

ρ is density; Y_i is unnormalised mol proportion and V_i is partial mol volume of each component i. V_i at pressure (P) and temperature (T) is given by

$$V_{i\ (at\ P\ and\ T)} = V_{i\ (at\ 0.1\ MPa\ and\ T)} + \frac{dV_i}{dT}(T - 1400°C) + \frac{dV_i}{dP}(P - 0.1MPa) \quad \text{(iii)}$$

dV_i/dT is thermal expansivity and dV_i/dP is compressibility. A variety of published data is used for the thermal expansivity and compressibility of metal oxides (Lange & Carmichael, 1987; Kress & Carmichael, 1991), H_2O (Lange, 1994; Ochs & Lange, 1999), P_2O_5 (Knoche *et al.*, 1995; Webb & Courtial, 1996) and CO_2 (Genge *et al.*, 1995b; Bourgue & Richet, 2001). There is some ambiguity over the thermal compressibility of CO_2 as the carbonate CO_3^{2-} ion: low thermal compressibility at low CO_2 concentrations in silicate magma at low pressure (Bourgue & Richet, 2001) versus high thermal compressibility in pure $CaCO_3$ magmas at high pressures (up to 10 GPa) (Genge *et al.*, 1995b). However, the melts under consideration are carbonated silicate magmas in the crust, such that the low pressure data (Bourgue & Richet, 2001) are most applicable.

Density modelling requires consideration of the volatile loss during ascent and emplacement of primitive mantle-derived melts. Published data sets (Nixon & Hornung, 1973; Woolley & Jones, 1987; Barker & Nixon, 1989; Bedard & Chown, 1992; Kalinkin *et al.*, 1993; Beard *et al.*, 1996; Riley *et al.*, 1996; Pracht & Kinnaird, 1997; Lapin *et al.*, 2005; Brady, 2010; Brady & Moore, 2012) for six well-described rock suites (volcanic or subvolcanic, silicocarbonatite and carbonated ultramafic lamprophyre lithologies) were used to extend the primary data set from

Ireland to a wide range of transitional carbonated silicate compositions. The published data are for rock suites in Germany, Scandinavia, Uzbekistan, Uganda, Malawi and Canada, which have variable nature and major element composition. However, all have features characteristic of parental magmas (isotopic signatures and transporting mantle-derived material), rather than aluminous or carbonate-rich magmas that assimilated crustal silica. In the first instance, the data were utilised to determine a molar ratio of dominant volatiles in primitive magmas.

Published whole-rock data that includes both CO_2 and H_2O (Nixon & Hornung, 1973; Woolley & Jones, 1987; Barker & Nixon, 1989) generates a (Vr) molar $CO_2/(CO_2 + H_2O)$ ratio of 0.80 ± 0.11 (1 s. d.). A similar volatile ratio is obtained where measured CO_2 and Loss on Ignition (LOI) data are published (Lapin *et al.*, 2005) and LOI-CO_2 data has been used as a proxy for bound H_2O. The scatter in data for Fort Portal is caused by the inclusion of analyses from volcanic rocks as well as subvolcanic rocks, and the relationship between carbonate content and density of magmas in subvolcanic settings is otherwise good (Fig. 5a). In contrast, silicocarbonatite melt inclusions that are trapped in plutonic calcite-carbonatite at Magnet Cove (Nesbitt & Kelly, 1977) have Vr = 0.60 (Fig. 5b). This indicates that the subvolcanic silicocarbonatite and lamprophyre magmas preferentially devolatilised H_2O relative to CO_2 during ascent, for little change in the major element composition of the primitive magma. Therefore, Vr conditions are constrained for modelling on the basis of increased dehydration of magmas from Vr = 0.60 in plutonic settings, to Vr = 0.75 for initial subvolcanic magmas and Vr = 0.86–0.92 for devolatilised subvolcanic and volcanic magmas. More recent melt inclusion studies do not present sufficient volatile data for modelling but Nielsen *et al.* (1997) provide corroboration that melt inclusion compositions are low-pressure fractionates of more magnesian larnite-normative ultramafic lamprophyre-type melts of primary mantle origin.

Table 3 and Fig. 5 shows the expected negative correlation between CO_2 concentration and magma density in a root zone complex of 81 MPa (equivalent to 2.5 km depth) and 900°C. The partial molar volume of CO_2 exists as the carbonate ion CO_3^{2-} and $CO_{2\,(mol)} > H_2O_{\,(mol)}$. Measured $CO_2 + H_2O$, or CO_2 + LOI (assumed to be equivalent to H_2O concentration) are used in calculations where the data are available, and molar $CO_2/(CO_2 + H_2O)$ or $Vr = 0.80 \pm 0.11$ (1 s. d.). LOI is assumed to represent total $CO_2 + H_2O$ where data are not available and Vr = 0.75 is used to provide meaningful initial volatile ratio in near-primitive parental magmas in subvolcanic settings. Application of a volatile ratio Vr = 0.75 to whole-rock analyses produces similar results for magma density as calculations including measured volatile ratios, despite variations in major element composition, such that volatile concentration is the dominant control on magma density in transitional magmas. There is an expected

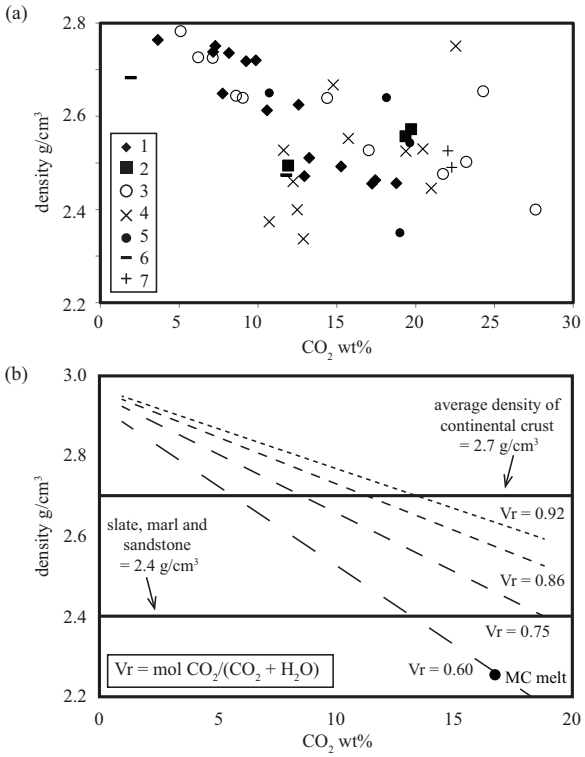

Fig. 5. Variation in density of magma as a function of volatile content, where Vr = mol $CO_2/(CO_2 + H_2O)$. Conditions used for density calculation are 900°C and 2.5 km depth (81 MPa). (a) Density of magma as a function of measured and inferred volatile concentrations in whole-rock analyses: Vr is calculated for localities 3–5; a Vr = 0.75 is applied to LOI for other localities*. An error in estimation of temperature of ±100°C will result in an error of <0.02 g/cm³. (b) Density of magma as a function of the volatile ratio, using Beara suite of analyses as a proxy for major element compositions. Crustal densities and the density calculated for the composition of melt inclusions from the Magnet Cove (MC) carbonatite (Nesbitt & Kelly, 1977) are shown for reference. *Whole-rock data are from the following localities: 1, Beara Peninsula, Co. Cork, Ireland (Pracht & Kinnaird, 1997; Brady, 2010; Brady & Moore, 2012); 2, Auf Dickel, Rockeskyll, Germany (Riley *et al.*, 1996); 3, Chagatai, Uzbekistan (Lapin *et al.*, 2005); 4, Fort Portal, Uganda (Nixon & Hornung, 1973; Barker & Nixon, 1989); 5, Chilwa, Malawi (Woolley & Jones, 1987); 6, Kola Peninsula (Kalinkin *et al.*, 1993; Beard *et al.*, 1996); and 7, Abitibi, Canada (Bedard & Chown, 1992).

negative correlation between CO_2 concentration and melt density for natural rock compositions. The most significant error in the model arises from the estimate of magma temperature but this is not considered significant for density calculations, given that a variation of ±100°C produces a change in density of less than 0.02 g/cm³.

A significant increase in magma density of 0.2 g/cm³ is caused by 50% dehydration from a deep emplacement level (Vr = 0.60) to a shallow emplacement level (Vr = 0.75) for magmas with $10 < CO_2$ wt% < 20 (Fig. 5b). The instantaneous exsolution of volatiles from low viscosity magmas is confirmed by autometasomatism of xenoliths in sills of the Beara Peninsula (Fig. 2e) at the point of sill inception and decrease in magmatic overpressure. Even though the most hydrated silicocarbonatite magmas (Vr < 0.75) remain positively buoyant relative to continental crust (Fig. 5b), rheological contrasts and the stress regime in the crust will promote sill formation (Menand, 2011). The estimate of Vr prior to the

instant of sill formation is 0.60, since the plutonic context (MC; Fig. 5b) is comparable with the magma density calculated for the Beara lithologies prior to devolatilisation.

CRYSTAL SETTLING

Sill inception, such as that observed in the Beara Peninsula, followed by incremental inflation is cited as a general mechanism for the growth of magma chambers (Kavanagh *et al.*, 2006, 2015; Menand, 2011). Entrainment in a magma chamber is described by wd/v, where w is the inflow velocity of a recharging magma from a feeder dyke of width d, into a magma of viscosity v (Campbell & Turner, 1986). Carbonatite that ascends rapidly and turbulently through a wide-enough feeder dyke may entrain a higher viscosity magma (Moore *et al.*, 2009). However, with an increase in viscosity with cooling of the magma during ascent and a wd/v that will usually be <7, it is more likely that carbonatite magma will spread in a thin sheet at the bottom of a carbonatite magma chamber (Valentini *et al.*, 2010). We use a sheet-shaped and inflating silicocarbonatite magma body to postulate on the nature of crystal settling.

Where small incremental injections of silicocarbonatite magmas move along the base of a tabular magma chamber, laminar flow is likely and Reynold's number is reduced. Stoke's Law settling is then a valid means to approximate crystal settling, modified for crystal shape using the shape factor S_e (Kerr & Lister, 1991). Initial Stoke's Law modelling inputs include a crystal size of 1 mm, phlogopite shape factor S_e of 0.67, apatite shape factor S_e of 0.76, an intrusive depth of 2.5 km, an emplacement temperature of 900°C and a Vr = 0.6. Olivine, pyroxene and magnetite settling is not significantly affected by the CO_2 concentration of magmas: minimum settling rates are 0.4 cm/sec for olivine and pyroxene, and 1.5 cm/sec for magnetite.

The results deviate significantly from the rapid settling of an entire mineral assemblage previously modelled for silica-absent end-member carbonatite magma emplaced in one event into a cylindrical chamber (Treiman & Schedl, 1983). Under the conditions of an inflating chamber of primitive carbonated silicate liquids, calcite will float and flotation of phlogopite also becomes possible at low CO_2 contents and higher Vr (Fig. 6a). Crystal shape influences the phlogopite and apatite settlement rates: thin books of phlogopite will preferentially float in liquids; recently nucleated and immature apatite will settle more slowly. The flotation of calcite is promoted by dehydration of the magma and the critical CO_2 concentration at which calcite (± phlogopite) will float is 10 wt% for Vr = 0.6; approaching 13 wt% for Vr = 0.92 (Fig. 6b).

The critical CO_2 concentration at which flotation occurs was determined in this study for rheological properties of hydrated magmas (Table 3). However, the loss of fluorine, chlorine and alkali metals may also play a role in the concentration of CO_2 at which a

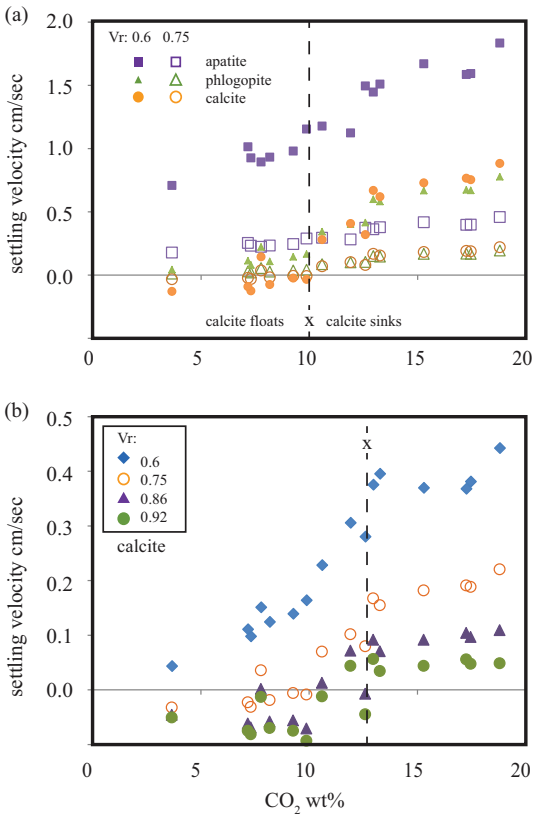

Fig. 6. Settling rates of apatite, phlogopite and calcite as a function of CO_2 concentration in magma at 900°C and 81 MPa. (a) All minerals sink in carbonated magmas with high water content. The settling rates for all minerals are lowest in dehydrated magmas (e.g. Vr = 0.75). Phlogopite tends towards neutral buoyancy and calcite floats at the critical CO_2 concentration x = 10 wt% CO_2 (dashed line). (b) The critical CO_2 concentration at which calcite floats (x) is extended towards 13 wt% CO_2 by continued dehydration of the magma to Vr = 0.92.

flotation mineral assemblage forms. We did not account for the effect of mineral attachment on fluid bubbles, which is known to assist magnetite flotation in silicate magmas (Edmonds *et al.*, 2015; Knipping *et al.*, 2019). Attachment onto bubbles is very likely to accelerate flotation of calcite, apatite and silicate minerals but the higher density contrast between carbonatite magma and magnetite may yet preclude magnetite flotation. Cooling simply slowed settling rate and pressure variation did not affect the range of liquid compositions over which calcite ± phlogopite will float. An increase in grain size increases the efficiency of separation between cumulate layers and flotation assemblages as long as CO_2 concentration is <13 wt%.

MODEL OF A RECHARGING SILICOCARBONATITE MAGMA CHAMBER

The model is premised on the geological field observations and the results of modelling. A sketch is presented (Fig. 7) of the geometrical instance where a sill inflates to become an initial crystallising magma body. New pulses of primitive magma spread out in a thin sheet across the base, with a reduction in magmatic overpressure

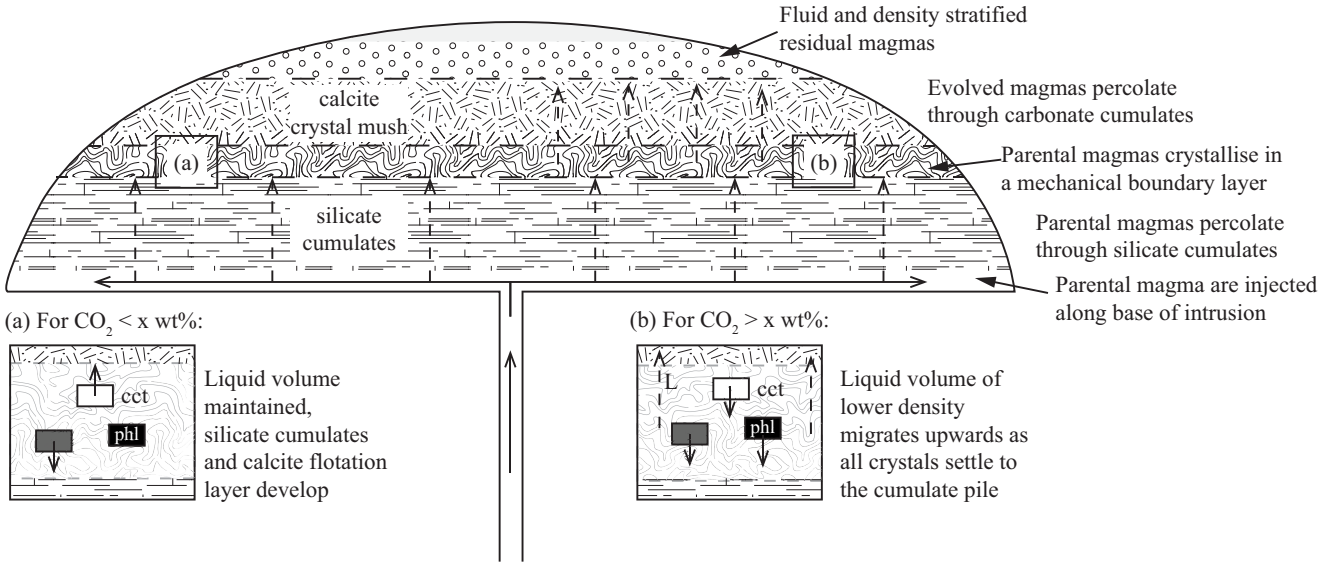

Fig. 7. Model of a density stratified silicocarbonatite magma chamber, with the geometry of an inflating sill. The settling regime is controlled by x, the critical CO_2 concentration at which a flotation assemblage forms, and by Vr. In scenario (a), the volume in a mechanical boundary layer is maintained by repeated injections of dehydrating primitive magma that percolate through cumulates and flotation of calcite. In scenario (b), the mechanical boundary layer is no longer sustained by new pulses of magma injection and all magma in the mechanical boundary layer evolves and migrates upwards through the flotation assemblage.

and concomitant reduction in PH_2O of the magma. The injected CO_2-rich magma and exsolved volatiles percolate easily through the growing silicate cumulate pile. Magmas accumulate between the cumulate pile and the calcite-dominated flotation assemblage (or crystal mush) due to their intermediate density. Thus, a mechanical boundary layer is created where a density filtering system will operate. Only highly evolved CO_2-rich magmas can percolate through the upper carbonate flotation cumulate pile. The mechanical boundary layer is insulated by both the cumulate and flotation assemblages and the latent heat of crystallisation is retained, in contrast to individual small-volume, carbonate magmas with low heat capacity. Very significantly, repeated replenishment by relatively small fraction melts into a maintained and crystallising magmatic layer provides a mechanism to (1) incrementally create a large carbonatite intrusion from small pulses of carbonated magma from metasomatically enriched mantle; (2) pre-concentrate incompatible elements, such as the Large Ion Lithophile Elements (LILE) and REEs that are characteristic of late-stage carbonatites.

Silicate cumulates will be dominated by pyroxenite or phoscorite (olivine/diopside-magnetite-apatite-phlogopite rocks), depending on flotation of phlogopite (Fig. 2), both of which are characteristically associated with calcite-carbonatite intrusions (Woolley & Kjarsgaard, 2008). A thickening cumulate pile of dense ultramafic minerals would simultaneously displace the mechanical boundary layer and the flotation assemblage upwards. The upwards stress on the flotation calcite layer, in conjunction with the lower density of the calcite mush, would promote vertical plastic injection of a crystal-rich carbonatite mush. In this model, a low density calcite crystal mush might ascend further through the crust in suitable stress regimes, and a calcite-carbonatite complex might have no apparent silicate rock association (Woolley & Kjarsgaard, 2008).

The compacting cumulate pile would also load the underlying crust and the local stress field could eventually inhibit magmatic injection and recharge. Where the magma evolution rate exceeds replenishment rate in the magma chamber, then CO_2 concentration in the magma will increase as a function of closed system crystallisation of silicate minerals and magma density will be reduced. When calcite ± phlogopite flotation can no longer be sustained in low density magmas, then incompatible element-enriched residual magmas will filter upwards, metasomatising the carbonatite flotation assemblage, i.e. autometasomatism will occur due to the percolation of paramagmatic fluids (Elliott *et al.*, 2018; Yaxley *et al.*, 2022).

Transfer of small volumes of parental magma to an injection site with a more conducive local stress field could repeat the processes of magma ponding and evolution, resulting in complex multi-stage magmatic and metasomatic relations. Variable rock associations and multiple generations of metasomatic overprinting, in combinations unique to the evolving local stress regime, are characteristic of calcite-carbonatite complexes. Our model is a potential precursor to diapirically-emplaced pairings of phoscorite and carbonatite arising from multiple intrusions/injections of partially crystallised magmatic masses, with PGE enrichment more normally associated with ultramafic layered intrusions (Fontana, 2006).

CONCLUDING COMMENTS

The rheological properties for natural parental silicocarbonantite magmas, not previously available for magmatic modelling, are determined. Silicocarbonatite has a lower density and higher viscosity than that previously modelled for pure end-member carbonate liquids. Silicocarbonatite liquids will nevertheless ascend rapidly along fault-facilitated pathways, perhaps assisted by decrease in silica activity at the point of 'take off' (Bailey, 1985; Woolley & Bailey, 2012; Massuyeau *et al.*, 2015). There is a preservation bias of silicocarbonatites towards subvolcanic and explosive emplacement because the magmas that are arrested at rheological barriers in the crust evolve to form cumulates, immiscible liquids and residual fluids, which may interact extensively with crustal host rocks. The dehydration accompanying ponding of silicocarbonatite parental magmas increases crystallisation and molar $CO_2/(CO_2 + H_2O)$, promoting a mechanical and magmatic boundary layer between calcite-dominated flotation and silicate-dominated settlement cumulate mineral assemblages. Thermal capacity is maintained and open-system crystallisation concentrates incompatible elements prior to immiscibility- or fluid-dominated processes. The model provides a framework for consideration of the early evolution of parental magmas, for which there is scant evidence. The model represents a transitory scenario prior to further ascent of calcite-dominated crystal mush and separation of calcite-dominated and silicate-dominated lithologies. In particular, the model explains the volumetric disparity between the small fraction melts of metasomatised mantle and relatively large volumes of evolved magmas in carbonatite complexes and the variable rock associations observations in some natural carbonatite complexes.

ACKNOWLEDGMENTS

This modelling was inspired and funded by the European Union's Horizon 2020 research and innovation programme (grant agreement no. 689909: HiTech AlkCarb). For fieldwork and sample collection, K.R.M. and A.E.B. acknowledge funding from INTAS project 05-100008-7983 and the Irish Research Council for Science, Engineering and Technology. K. Ryan, C. Dempsey and S. Lavery are thanked for additional field assistance. F. Wall, B. Williamson, G. Rosatelli, J. Andersen and two anonymous reviewers are thanked for constructive comments.

References

Anenburg, M., Broom-Fendley, S. & Chen, W. (2021). Formation of rare earth deposits in carbonatites. *Elements* **17**, 327–332.

Anenburg, M. & Mavrogenes, J. A. (2018). Carbonatitic versus hydrothermal origin for fluorapatite REE-Th deposits: experimental study of REE transport and crustal "antiskarn" metasomatism. *American Journal of Science* **318**, 335–366.

Bailey, D. K. (1985). Fluids, melts, flowage and styles of eruption in alkaline ultramafic magmatism. *Transactions of the Geological Society of South Africa* **88**, 449–457.

Barker, D. S. & Nixon, P. H. (1989). High-Ca, low-alkali carbonatite volcanism at Fort Portal, Uganda. *Contributions to Mineralogy and Petrology* **103**, 166–177.

Beard, A. D., Downes, H., Vetrin, V., Kempton, P. D. & Maluski, H. (1996). Petrogenesis of Devonian lamprophyre and carbonatite minor intrusions, Kandalaksha Gulf (Kola Peninsula, Russia). *Lithos* **39**, 93–119.

Bedard, L. P. & Chown, E. H. (1992). The Dolodau dykes, Canada: an example of an Archean carbonatite. *Mineralogy and Petrology* **46**, 109–121.

Bottinga, Y. & Weill, D. F. (1970). Densities of liquid silicate systems calculated from partial molar volumes of oxide components. *American Journal of Science* **269**, 169–182.

Bourgue, E. & Richet, P. (2001). The effects of dissolved CO_2 on the density and viscosity of silicate melts: a preliminary study. *Earth and Planetary Science Letters* **193**, 57–68.

Brady, A. E. (2010) The role of carbonate in diatremic magmatism. Unpublished PhD thesis, National University of Ireland Galway, Ireland.

Brady, A. E. & Moore, K. R. (2012). A mantle-derived dolomite silicocarbonatite from the southwest coast of Ireland. *Mineralogical Magazine* **76**, 357–376.

Campbell, I. H. & Turner, J. S. (1986). The influence of viscosity on fountains in magma chambers. *Journal of Petrology* **27**, 1–30.

Chakmouradian, A.R. & Zaitsev, A. N. (2004). Afrikanda: an association of ultramafic, alkaline and alkali-silica-rich carbonatitic rocks from mantle- derived melts. In: Wall, Frances and Zaitsev, A. N. (ed.) *Phoscorites and Carbonatites from Mantle to Mine: the Key example of the Kola Alkaline Province*. Mineralogical Society Series, 10. London: Springer, 247–291.

Chmyz, L., Azzone, R. G., Ruberti, E., Marks, M. A. W. & Santos, T. J. S. (2022). Olivines as probes into assimilation of silicate rocks by carbonatite magmas: unraveling the genesis of reaction rocks from the Jacupiranga alkaline-carbonatite complex, southern Brazil. *Lithos* **416, 417**, 106647–106417.

Dalton, J. A. & Presnall, D. C. (1998). Carbonatitic melts along the solidus of model lherzolite in the system CaO-MgO-Al 2 O 3 -SiO 2 -CO 2 from 3 to 7 GPa. *Contributions to Mineralogy and Petrology* **131**, 123–135.

Dalton, J. A. & Wood, B. J. (1993). The compositions of primary carbonate melts and their evolution through wallrock reaction in the mantle. *Earth and Planetary Science Letters* **119**, 511–525.

Daniels, K. A., Kavanagh, J. L., Menand, T., Sparks, R. S. J., Campus, C. & Road, W. (2012). The shapes of dikes: evidence for the influence of cooling and inelastic deformation. *Bulletin of the Geological Society of America* **124**, 1102–1112.

Demény, A. & Harangi, S. (1996). Stable isotope studies and processes of carbonate formation in Hungarian alkali basalts and lamprophyres: evolution of magmatic fluids and magma-sediment interactions. *Lithos* **37**, 335–349.

Dobson, D. P., Jones, A. P., Rabe, R., Sekine, T., Kurita, K., Taniguchi, T., Kondo, T., Kato, T., Shimomura, O. & Urakawa, S. (1996). In-situ measurement of viscosity and density of carbonate melts at high pressure. *Earth and Planetary Science Letters* **143**, 207–215.

Drüppel, K., Hoefs, J. & Okrusch, M. (2005). Fenitizing processes induced by ferrocarbonatite magmatism at Swartbooisdrif, NW Namibia. *Journal of Petrology* **46**, 377–406.

Edmonds, M., Brett, A., Herd, R. A., Humphreys, M. C. S. & Woods, A. (2015). Magnetite-bubble aggregates at mixing interfaces in

andesite magma bodies. *Geological Society Special Publication* **410**, 95–121.

Elliott, H. A. L., Wall, F., Chakhmouradian, A. R., Siegfried, P. R., Dahlgren, S., Weatherley, S., Finch, A. A., Marks, M. A. W., Dowman, E. & Deady, E. (2018). Fenites associated with carbonatite complexes: a review. *Ore Geology Reviews* **93**, 38–59.

Fontana, J. (2006). Phoscorite-Carbonatite pipe complexes. *Platinum Metals Review* **50**, 134–142.

Freestone, I. C. & Hamilton, D. L. (1980). The role of liquid immiscibility in the genesis of carbonatites - an experimental study. *Contributions to Mineralogy and Petrology* **73**, 105–117.

Genge, M. J., Jones, A. P. & Price, G. D. (1995a). An infrared and Raman study of carbonate glasses: implications for the structure of carbonatite magmas. *Geochimica et Cosmochimica Acta* **59**, 927–937.

Genge, M. J., Price, G. D. & Jones, A. P. (1995b). Molecular dynamics simulations of $CaCO_3$, melts to mantle pressures and temperatures: implications for carbonatite magmas. *Earth and Planetary Science Letters* **131**, 225–238.

Gernon, T. M., Gilbertson, M. A., Sparks, R. S. J. & Field, M. (2009). The role of gas-fluidisation in the formation of massive volcaniclastic kimberlite. *Lithos* **112**, 439–451.

Giebel, R. J., Parsapoor, A., Walter, B. F., Braunger, S., Marks, M. A. W., Wenzel, T. & Markl, G. (2019). Evidence for Magma-Wall Rock interaction in carbonatites from the Kaiserstuhl Volcanic Complex (Southwest Germany). *Journal of Petrology* **60**, 1163–1194.

Giordano, D., Russell, J. K. & Dingwell, D. B. (2008). Viscosity of magmatic liquids: a model. *Earth and Planetary Science Letters* **271**, 123–134.

Girnis, A. V., Bulatov, V. K. & Brey, G. P. (2005). Transition from kimberlite to carbonatite melt under mantle parameters: an experimental study. *Petrology* **13**, 1–15.

Gittins, J. (1989) The origin and evolution of carbonatite magmas. In: (Bell K. (ed)) *Carbonatites-Genesis and Evolution*. London: Unwin Hyman, pp.580–600.

Govindaraju, K. (1994). 1994 compilation of working values and sample description for 383 geostandards. *Geostandards and Geoanalytical Research* **18**, 1–158.

Green, D. H. & Wallace, M. E. (1988). Mantle metasomatism by ephemeral carbonatite melts. *Nature* **336**, 459–462.

Gudfinnsson, G. H. & Presnall, D. C. (2005). Continuous gradations among primary carbonatitic, kimberlitic, melilititic, basaltic, picritic and komatiitic melts in equilibrium with garnet lherzolite at 3-8 GPa. *Journal of Petrology* **46**, 1645–1659..

Harmer, R. E. & Gittins, J. (1997). The origin of dolomitic carbonatites: field and experimental constraints. *Journal of African Earth Sciences* **25**, 5–28.

Hegner, E., Rajesh, S., Willbold, M., Müller, D., Joachimski, M., Hofmann, M., Linnemann, U., Zieger, J. & Pradeepkumar, A. P. (2020). Sediment-derived origin of the putative Munnar carbonatite, South India. *Journal of Asian Earth Sciences* **200**, 104432.

Hort, M. (1998). Abrupt change in magma liquidus temperature because of volatile loss or magma mixing: effects on nucleation, crystal growth and thermal history of the magma. *Journal of Petrology* **39**, 1063–1076.

Hunter, R. H. & McKenzie, D. (1989). The equilibrium geometry of carbonate melts in rocks of mantle composition. *Earth and Planetary Science Letters* **92**, 347–356.

Kalinkin, M. M., Arzamastsev, A. A. & Polyakov, I. V. (1993). Kimberlites and related rocks of the Kola Region. *Petrology* **1**, 173–180.

Kamenetsky, V. S., Doroshkevich, A. G., Elliott, H. A. L. & Zaitsev, A. N. (2021). Carbonatites: contrasting, complex, and controversial. *Elements* **17**, 307–314.

Kavanagh, J. L., Boutelier, D. & Cruden, A. R. (2015). The mechanics of sill inception, propagation and growth: experimental evidence for rapid reduction in magmatic overpressure. *Earth and Planetary Science Letters* **421**, 117–128.

Kavanagh, J. L., Menand, T. & Sparks, R. S. J. (2006). An experimental investigation of sill formation and propagation in layered elastic media. *Earth and Planetary Science Letters* **245**, 799–813.

Keller, J. & Hoefs, J. (1995). Stable isotope characteristics of recent natrocarbonatites from Oldoinyo Lengai. In: Bell K K. J. (ed.) *Carbonatite Volcanism*. Berlin, Heidelberg: Springer, 113–123

Kerr, R. C. & Lister, J. R. (1991). The effects of shape on crystal settling and on the rheology of magmas. *The Journal of Geology* **99**, 457–467.

Knipping, J. L., Webster, J. D., Simon, A. C. & Holtz, F. (2019). Accumulation of magnetite by flotation on bubbles during decompression of silicate magma. *Scientific Reports* **9**, 3852–3857.

Knoche, R., Dingwell, D. B. & Webb, S. L. (1995). Melt densities for leucogranites and granitic pegmatites: partial molar volumes for SiO2, Al2O3, Na2O, K2O, Li2O, Rb2O, Cs2O, MgO, CaO, SrO, BaO, B2O3, P2O5, F2O−1, TiO2, Nb2O5, Ta2O5, and WO3. *Geochimica et Cosmochimica Acta* **59**, 4645–4652.

Kono, Y., Kenney-Benson, C., Hummer, D., Ohfuji, H., Park, C., Shen, G., Wang, Y., Kavner, A. & Manning, C. E. (2014). Ultralow viscosity of carbonate melts at high pressures. *Nature Communications*, Nature Publishing Group **5**, 2–5.

Kress, V. C. & Carmichael, I. S. E. (1991). The compressibility of silicate liquids containing Fe2O3 and the effect of composition, temperature, oxygen fugacity and pressure on their redox states. 82–92.

Lange, R. A. (1994). The effect of H_2O, CO_2 and F on the density and viscosity of silicate melts. *Reviews in Mineralogy and Geochemistry* **30**, 331–369.

Lange, R. A. & Carmichael, I. S. E. (1987). Densities of Na2O-K2O-CaO-MgO-FeO-Fe2O3-Al2O3-TiO2-SiO2 liquids: new measurements and derived partial molar properties. *Geochimica et Cosmochimica Acta* **51**, 2931–2946.

Lapin, A. V., Divaev, F. K. & Kostityn, Y. A. (2005). Petrochemical interpretation of carbonatite-like rocks from the Chagatai Complex of the Tien Shan with application to the problem of diamond potential. *Petrology* **13**, 499–511.

Lee, W.-J. & Wyllie, P. J. (1997). Liquid immiscibility between nephelinite and carbonatite from 1.0 to 2.5 GPa compared with mantle melt compositions. *Contributions to Mineralogy and Petrology* **127**, 1–16.

Masson, C. R. (1972). Thermodynamics and constitution of silicate slags. *Journal of the Iron Steel Industry* **210**, 89–96.

Masson, C. R., Smith, I. B. & Whiteway, S. G. (1970). Activities and ionic distributions in liquid silicates: application of polymer theory. *Canadian Journal of Research Section B, Chemical Sciences* **48**, 1456–1464.

Massuyeau, M., Gardés, E., Morizet, Y. & Gaillard, F. (2015). A model for the activity of silica along the carbonatite-kimberlite-mellilitite-basanite melt compositional joint. *Chemical Geology* **418**, 206–216.

Menand, T. (2011). Physical controls and depth of emplacement of igneous bodies: a review. *Tectonophysics* **500**, 11–19.

Middlemost, E. (1990). Mineralogy and petrology of the rauhaugites of the Mt Weld Carbonatite Complex of Western Australia. *Mineralogy and Petrology* **41**, 145–161.

Mitchell, R. H. (2005). Carbonatites and carbonatites and carbonatites. *The Canadian Mineralogist* **43**, 2049–2068.

Moore, K. R. (2012). Experimental study in the Na2O–CaO–MgO–Al2O3–SiO2–CO2system at 3 GPa: the effect of sodium on

mantle melting to carbonate-rich liquids and implications for the petrogenesis of silicocarbonatites. *Mineralogical Magazine* **76**, 285–309.

Moore, K. R. & Wood, B. J. (1998). The transition from carbonate to silicate melts in the CaO–MgO–SiO2–CO2 system. *Journal of Petrology* **39**, 1943–1951.

Moore, K. R., Wall, F., Divaev, F.K. & Savatenko, V.M. (2009). Mingling of carbonate and silicate magmas under turbulent flow conditions: evidence from rock textures and mineral chemistry in sub-volcanic carbonatite dykes, Chagatai, Uzbekistan. *Lithos* **110**, 65–82.

Nesbitt, B. E. & Kelly, W. C. (1977). Magmatic and hydrothermal inclusions in carbonatite of the Magnet Cove Complex, Arkansas. *Contributions to Mineralogy and Petrology* **63**, 271–294.

Nielsen, T. F. D., Solovova, I. P. & Veksler, I. V. (1997). Parental melts of melilitolite and origin of alkaline carbonatite: evidence from crystallised melt inclusions, Gardiner Complex. *Contributions to Mineralogy and Petrology* **126**, 331–344.

Nixon, P. H. & Hornung, G. (1973). The carbonatite lavas and tuffs near Fort Portal. Western Uganda. *Overseas Geology and Mineral Resources* **41**, 168–179.

Ochs, F. A. & Lange, R. A. (1999). The density of hydrous magmatic liquids. *Science* **283**, 1314–1317.

Pracht, M. (1994) The geology of the Beara Peninsula, Ireland. Unpublished PhD thesis, National University of Ireland, Cork, Ireland.

Pracht, M. & Kinnaird, J. A. (1995). Mineral chemistry of megacrysts and ultramafic nodules from an undersaturated pipe at Black Ball Head, County Cork. *Irish Journal of Earth Sciences* **14**, 47–58.

Pracht, M. & Kinnaird, J. A. (1997). Carboniferous subvolcanic activity on the Beara Peninsula, SW Ireland. *Geological Journal* **32**, 297–312.

Pracht, M. & Timmerman, M. J. (2004). A late Namurian (318 Ma) 40Ar/39Ar age for kaersutite megacrysts from the Black Ball Head diatreme: an age limit for the Variscan deformation in South-West Ireland. *Irish Journal of Earth Sciences* **22**, 33–43.

Quinn, D., Meere, P. A. & Wartho, J. (2005). A chronology of foreland deformation: ultra-violet laser $^{40}Ar/^{39}Ar$ dating of syn/late-orogenic intrusions from the Variscides of Southwest Ireland. *Journal of Structural Geology* **27**, 1413–1425.

Riley, T. R., Bailey, D. K. E. N. & Lloyd, F. E. (1996). Extrusive carbonatite from the Quaternary Rockeskyll Complex, West Eifel, Germany. *The Canadian Mineralogist* **34**, 389–401.

Rock, N. M. S. (1987). The nature and origin of lamprophyres: an overview. In: J.G. Fitton (ed.) *Geological Society, London, Special Publications*. Geological Society Special Publication **30**, 191–226.

Rock, N. M. S. (1991) *Lamprophyres*. Glasgow: Blackie and Son Ltd.

Santos, R. V. & Clayton, R. N. (1995). The carbonate content in high-temperature apatite: an analytical method applied to apatite from the Jacupiranga alkaline complex. *American Mineralogist* **80**, 336–344.

Smith, M. P., Moore, K., Kavecsánszki, D., Finch, A. A., Kynicky, J. & Wall, F. (2016). From mantle to critical zone: a review of large and giant sized deposits of the rare earth elements. *Geoscience Frontiers* **7**, 315–334.

Stagno, V., Stopponi, V., Kono, Y., Manning, C. E. & Irifune, T. (2018). Experimental determination of the viscosity of Na_2CO_3 melt between 1.7 and 4.6 GPa at 1200–1700 °C: implications for the rheology of carbonatite magmas in the Earth's upper mantle. *Chemical Geology* **501**, 19–25.

Stoppa, F., Rukhlov, A. S., Bell, K., Schiazza, M. & Vichi, G. (2014). Lamprophyres of Italy: Early Cretaceous alkaline lamprophyres of southern Tuscany, Italy. *Lithos* **188**, 97–112.

Tappe, S., Foley, S. F., Jenner, G. A., Heaman, L. M., Kjarsgaard, B. A., Romer, R. L., Stracke, A., Joyce, N. & Hoefs, J. (2006). Genesis of ultramafic lamprophyres and carbonatites at Aillik Bay, Labrador: a consequence of incipient lithospheric thinning beneath the North Atlantic Craton. *Journal of Petrology* **47**, 1261–1315.

Taylor, H. P., Frechen, J. & Degens, E. T. (1967). Oxygen and carbon isotope studies of carbonatites from the Laacher See District, West Germany and the Alnö District, Sweden. *Geochimica et Cosmochimica Acta* **31**, 407–430.

Treiman, A. H. & Schedl, A. (1983). Properties of carbonatite magma and processes in carbonatite magma chambers. *The Journal of Geology* **91**, 437–447.

Valentini, L. & Moore, K. R. (2009). Numerical modeling of the development of small-scale magmatic emulsions by Korteweg stress driven flow. *Clinical and Laboratory Standards Institute (Series)* **179**, 87–95.

Valentini, L., Moore, K. R. & Chazot, G. (2010). Unravelling carbonatite-silicate magma interaction dynamics: a case study from the Velay province (Massif Central, France). *Lithos* **116**, 53–64.

Vichi, G., Stoppa, F. & Wall, F. (2005). The carbonate fraction in carbonatitic Italian lamprophyres. *Lithos* **85**, 154–170.

Vuilleumier, R., Seitsonen, A., Sator, N. & Guillot, B. (2014). Structure, equation of state and transport properties of molten calcium carbonate ($CaCO_3$) by atomistic simulations. *Geochimica et Cosmochimica Acta* **141**, 547–566.

Watkinson, D. H. & Wyllie, P. J. (1971). Experimental study of the composition join NaAlSiO4-CaCO3-H2O and the genesis of Alkalic Rock–Carbonatite Complexes. *Journal of Petrology* **12**, 357–378.

Webb, S. & Courtial, P. (1996). Compressibility of P_2O_5-Al_2O_3-Na_2SiO_3 melts. *Physics and Chemistry of Minerals* **23**, 205–211.

Weidendorfer, D., Schmidt, M. W. & Mattsson, H. B. (2017). A common origin of carbonatite magmas. *Geology* **45**, 507–510.

Wolff, J. A. (1994). Physical properties of carbonatite magmas inferred from molten salt data, and application to extraction patterns from carbonatite-silicate magma chambers. *Geological Magazine* **131**, 145–153.

Woolley, A. R. & Bailey, D. K. (2012). The crucial role of lithospheric structure in the generation and release of carbonatites: geological evidence. *Mineralogical Magazine* **76**, 259–270.

Woolley, A. R. & Jones, G. C. (1987). The petrochemistry of the northern part of the Chilwa Alkaline Province, Malawi. In: Fitton, J. G. & Upton, B. G. J. (eds) *Geological Society, London, Special Publications*. Geological Society Special Publication 30, 335–355,

Woolley, A. R. & Kjarsgaard, B. A. (2008). Paragenetic types of carbonatite as indicated by the diversity and relative abundances of associated silicate rocks: evidence from a global database. *The Canadian Mineralogist* **46**, 741–752.

Yaxley, G. M., Anenburg, M., Tappe, S., Decree, S. & Guzmics, T. (2022). Carbonatites: classification, sources, evolution, and emplacement. *Annual Review of Earth and Planetary Sciences* **50**, 261–293.

Yaxley, G. M., Kjarsgaard, B. A. & Jaques, A. L. (2021). Evolution of carbonatite magmas in the upper mantle and crust. *Elements* **17**, 315–320.